Supplemental Materials for Hidden charge order in an iron oxide square-lattice compound

Jung-Hwa Kim,[1,*] Darren C. Peets,[1,2,3,*] Manfred Reehuis,[4] Peter Adler,[5] Andrey Maljuk,[1,6] Tobias Ritschel,[3] Morgan C. Allison,[3] Jochen Geck,[3,7] Jose R. L. Mardegan,[8] Pablo J. Bereciartua Perez,[8] Sonia Francoual,[8] Andrew C. Walters,[1] Thomas Keller,[1,9] Paula M. Abdala,[10] Philip Pattison,[10,11] Pinder Dosanjh,[12] and Bernhard Keimer[1,†]

[1] *Max-Planck-Institut für Festkörperforschung, D-70569 Stuttgart, Germany*
[2] *Ningbo Institute for Materials Technology and Engineering, Chinese Academy of Sciences, Zhenhai, Ningbo, 315201 Zhejiang, China*
[3] *Institut für Festkörper- und Materialphysik, Technische Universität Dresden, D-01069 Dresden, Germany*
[4] *Helmholtz-Zentrum Berlin für Materialien und Energie, D-14109 Berlin, Germany*
[5] *Max-Planck-Institut für Chemische Physik fester Stoffe, D-01187 Dresden, Germany*
[6] *Leibniz Institut für Festkörper- und Werkstoffforschung, D-01171 Dresden, Germany*
[7] *Würzburg-Dresden Cluster of Excellence ct.qmat, Technische Universität Dresden, 01062 Dresden, Germany*
[8] *Deutsches Elektronen-Synchrotron DESY, Hamburg 22603, Germany*
[9] *Max Planck Society Outstation at the Heinz Maier-Leibnitz Zentrum (MLZ), D-85748 Garching, Germany*
[10] *SNBL at ESRF, BP 220, F-38042 Grenoble Cedex 9, France*
[11] *Laboratory for Quantum Magnetism, École polytechnique fédérale de Lausanne (EPFL), BSP-Dorigny, CH-1015 Lausanne, Switzerland*
[12] *Department of Physics and Astronomy, University of British Columbia, Vancouver, BC, V6T 1Z1 Canada*

CRYSTAL GROWTH AND CHARACTERIZATION

High-quality single crystalline rods of $Sr_3Fe_2O_7$ grown by the floating zone technique [1, 2] were annealed to full oxygen stoichiometry following two different temperature programs: The material studied here by Mössbauer spectroscopy, resistivity, neutron diffraction, Larmor diffraction, and synchrotron powder diffraction was annealed under 6 kbar of oxygen pressure at 550°C for 100 h then cooled slowly to room temperature. Crystals used for resonant x-ray diffraction and synchrotron single-crystal diffraction were annealed for 48 hours at 450°C in 5 kbar of oxygen to rapidly oxygenate the sample, cooled to 400°C in 6 hours and held there for 24 hours to ensure equilibrium, cooled to 350°C in 96 hours then to 275 in 48 hours to maximize the oxygen content, then cooled to room temperature in an additional 24 hours. Specific heat measurements were performed on both sets of samples and were indistinguishable, so these were averaged. The oxygen contents were verified by thermogravimetry, and by refinement of diffraction data. Thermogravimetric analysis indicated an oxygen content of 6.92 for the former annealing program and 6.96 for the latter, both within the uncertainty of 7.00, and additionally showed a glitch on warming at 332(5) K, consistent with the charge-order transition.

The specific heat was measured on single crystals of $Sr_3Fe_2O_7$ in a Quantum Design Physical Properties Measurement System (PPMS), in zero field and for fields up to 9 T along the c axis. No hysteresis nor field dependence was observed above the magnetic transition, and as mentioned above, measurements on crystals from the two batches were indistinguishable and were averaged. Samples were attached to the sample holder using Apiezon N grease for measurements below 200 K; Apiezon H grease was used for higher-temperature measurements to avoid the glass transition of Apiezon N grease. Resistivity was measured in standard four-probe geometry in a Quantum Design PPMS. Gold wires were attached with silver epoxy, which was allowed to cure for several hours at 180–200°C in air before the crystal was mounted to the sample puck with GE Varnish. Thermogravimetric analysis had previously indicated that at these temperatures the oxygen mobility remains extremely low, the oxygen content does not change, and any intercalated water tends to deintercalate, ensuring that the resistivity samples were not altered or damaged while curing the epoxy.

NEUTRON DIFFRACTION

Single-crystal neutron diffraction was performed on the four-circle diffractometer E5 at the BER-II reactor (Helmholtz-Zentrum Berlin, Germany) using the neutron wavelength 0.896 Å. Refinements were carried out with the program Xtal3.4 [3] using the nuclear scattering lengths $b(\mathrm{O}) = 5.805$ fm, $b(\mathrm{Fe}) = 9.54$ fm, and $b(\mathrm{Sr}) = 7.02$ fm [4]. A data set of 1302 reflections (303 unique) was collected at 390 K, well above T_{CO}. Refinements of a total of 19 parameters (i.e., the overall scale and extinction factors, 4 positional parameters, and 13 anisotropic thermal parameters) in the space group $I4/mmm$ showed no indications of any reduction in symmetry. Data taken below the charge order transition showed no change.

NONRESONANT X-RAY DIFFRACTION

To determine the crystal structure for $T < T_{CO}$, high-resolution synchrotron powder diffraction measurements were performed at the BM01B (Swiss-Norwegian) beamline at the ESRF (Grenoble, France) using the wavelength $\lambda = 0.5035$ Å. The data were refined using the program FULLPROF [5], using the atomic scattering factors provided therein. However, no peak splittings or additional superstructure reflections were observed. The search for weak superstructure reflections continued at beamline BM01A at the ESRF, using a $\sim$10 μm-diameter $Sr_3Fe_2O_7$ single crystal. Data were collected with a Pilatus area detector, using the photon wavelength 0.6973 Å.

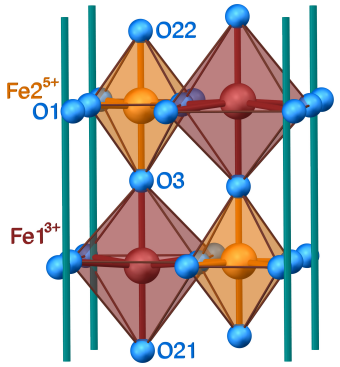

FIG. S1. Labelling of the crystallographic sites in the charge-ordered phase. The distortions are exaggerated for clarity.

TABLE I. Results of the crystal structure refinement of $Sr_3Fe_2O_7$ from single-crystal neutron diffraction data (λ = 0.89 Å) collected at 390 K. The refinement was carried out in the tetragonal space group $I4/mmm$, resulting in a residual $R_F = 0.068$. The thermal parameters U_{ij} (given in 100 Å^2) are in the form $\exp\left[-2\pi^2\left(U_{11}h^2(a^*)^2 + ...2U_{13}hla^*c^*\right)\right]$. For symmetry reasons, in $I4/mmm$ the values U_{11} and U_{22} are identical for the atoms Sr1, Sr2, Fe, O1 and O3, and all parameters U_{12}, U_{13} and U_{23} are equal to zero. O1 is equatorial, O2 is apical, and O3 is the shared apical oxygen in the center of the bilayer.

	Site	x	y	z	U_{11}	U_{22}	U_{33}	Occ
Sr1	2b	0	0	$\frac{1}{2}$	1.32(8)	1.32	1.03(8)	1
Sr2	4e	0	0	0.31656(8)	1.64(6)	1.64	0.97(6)	1
Fe	4e	0	0	0.09745(6)	0.79(4)	0.79	0.70(5)	1
O1	8g	0	$\frac{1}{2}$	0.09432(8)	1.52(8)	1.33(7)	1.23(5)	1
O2	4e	0	0	0.19309(11)	1.32(7)	1.32	0.99(6)	1
O3	2a	0	0	0	2.07(14)	2.07	1.64(13)	0.983(23)

$a = b = 3.846(4)$ Å, $c = 20.234(2)$ Å, $V = 299.4(6)$ Å^3

TABLE II. Results of the crystal structure refinements of $Sr_3Fe_2O_7$ from high-resolution synchrotron powder diffraction data ($\lambda = 0.5035$ Å) collected at 15 K. The refinements were carried out in the orthorhombic space group $Bmmb$. The parameter z(O3) was not allowed to vary, and the thermal parameters B were constrained to be identical for each element.

$Bmmb$	Site	x	y	z	B (Å^2)
Sr1	4c	0	$\frac{3}{4}$	0.2500(12)	0.290(4)
Sr21	4c	0	$\frac{3}{4}$	0.4330(1)	0.290
Sr22	4c	0	$\frac{3}{4}$	0.0670(1)	0.290
Fe1	4c	0	$\frac{3}{4}$	0.6528(15)	0.306(10)
Fe2	4c	0	$\frac{3}{4}$	0.8471(15)	0.306
O1	16h	0.248(6)	0.505(5)	0.3450(1)	0.62(3)
O21	4c	0	$\frac{3}{4}$	0.5573(24)	0.62
O22	4c	0	$\frac{3}{4}$	0.9445(24)	0.62
O3	4c	0	$\frac{3}{4}$	$\frac{3}{4}$	0.62

$a = 5.43050(3)$ Å, $b = 5.43287(3)$ Å, $c = 20.12137(7)$ Å,

TABLE III. Fe–O bond lengths d in $Sr_3Fe_2O_7$ (in Å) at 390 K, including the average bond length d_{av}.

$Sr_3Fe_2O_7$ at 390 K, in $I4/mmm$	
d(Fe–O1) ×4 (eq)	1.9244(22)
d(Fe–O2) ×1 (ap)	1.9352(26)
d(Fe–O3) ×1 (br)	1.9718(13)
d_{av}(Fe–O)	1.9341(21)

CRYSTALLOGRAPHIC PARAMETERS

The atomic coordinates resulting from refinements of neutron and synchrotron x-ray diffraction data at 390 and 15 K, respectively, are shown in Tables I and II, and the Fe–O bond lengths obtained at 390 K are given in Table III. Figure S1 indicates the labelling of the crystallographic sites. Somewhat enlarged standard deviations were obtained from synchrotron data for the positional parameters of the oxygen atoms in the low-temperature phase (Table II). This can be ascribed to the fact that these parameters are highly correlated, and to the fact that the scattering power of the oxygen atoms is relatively weak in x-ray diffraction.

The space group $Bmmb$ generates a general position 16h(x, y, z) for the equatorial O1 atoms. Here the three atomic positions could be individually refined; only the z parameter of O3 was fixed to be $z = 0.75$. Due to the enlarged standard deviations of the positional parameters of the oxygen atoms, it was not possible to determine individual bond lengths d(Fe–O) with good accuracy. However, we have obtained reasonable averaged bond lengths d_{av}(Fe1) = 1.950 Å and d_{av}(Fe2) = 1.917 Å.

NEUTRON LARMOR DIFFRACTION

High-resolution neutron Larmor diffraction data were taken at the resonant spin-echo triple-axis spectrometer TRISP at the FRM-II (Garching, Germany) with neutron wavevector 2.9 Å^{-1}. The crystal was aligned in the tetragonal (HHL) scattering plane and cooled in a closed-cycle refrigerator, and the tetragonal (2 2 0) and (0 0 10) nuclear Bragg peaks were investigated in zero applied field. The outgoing neutron polarization was measured as a function of the magnetic field applied along the incident and scattered neutron paths, parallel to the tetragonal (2 2 0) Bragg planes. The measured polarization data for the (2 2 0) peak are shown in Fig. S2.

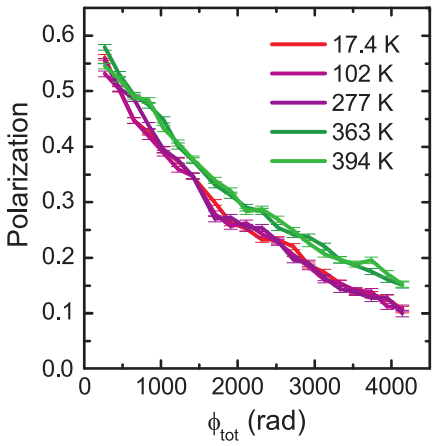

FIG. S2. Raw polarization data underpinning the neutron Larmor diffraction results on the tetragonal (2 2 0) peak. The increased depolarization at lower temperatures indicates a broadening of the lattice parameter.

RESONANT ELASTIC X-RAY SCATTERING

To enhance the contrast between the two Fe sites, we performed temperature-dependent single-crystal resonant elastic x-ray scattering (REXS) at the Fe K edge at beamline P09 at PETRA III (DESY, in Hamburg, Germany) [6], with the experimental geometry shown in the upper inset to Fig. S3(a). Before measurement, the sample was aligned using a Photonic Science Laue diffractometer with a tungsten source — the sharp diffraction spots, seen in the inset to Fig. S3(a), indicate the high quality of the single crystal. The Laue pattern produced no clear evidence for superstructure reflections. The sample was mounted on the cold finger of a closed-cycle displex cryostat sitting in a six-circle diffractometer, with the (0 0 1) axis in the vertical scattering plane; σ polarization was used. An avalanche photodiode point detector was used to measure the scattered x-ray intensity, and a VORTEX Si-drift diode fluorescence detector was employed to measure the total fluorescence yield (TFY) from the sample. Fig. S3(a) shows the TFY of $Sr_3Fe_2O_7$ measured as a function of the incident photon energy across the Fe K edge. The main edge at around 7128 eV and a small pre-edge at around 7115 eV are clearly visible.

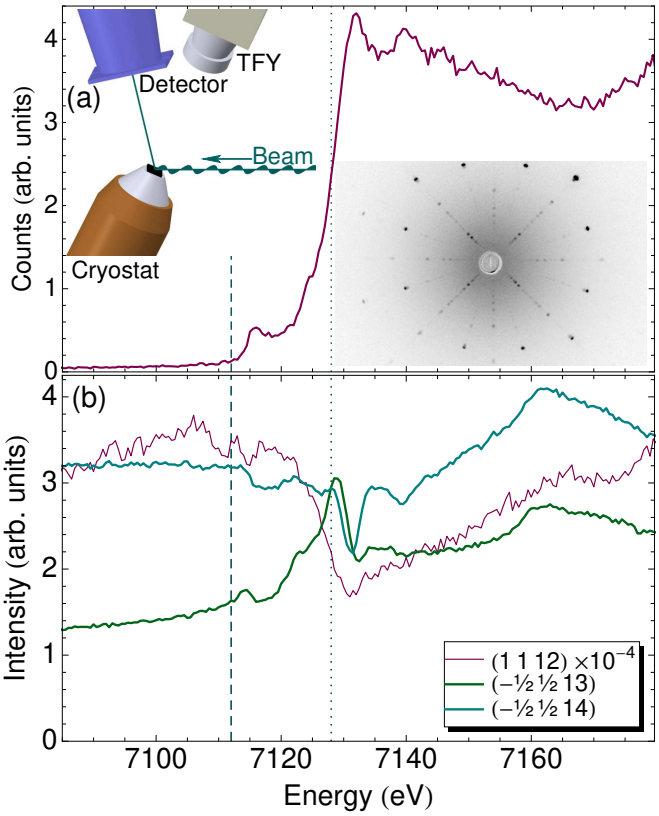

FIG. S3. (a) X-ray absorption spectrum of $Sr_3Fe_2O_7$ at the Fe K edge, from total fluorescence yield measurements. The dashed line indicates the beam energy of 7112 eV used for the temperature-dependent data in the main text while the dotted line identifies the on-resonant energy whose L-dependence is fit in Fig. 4(b). The left inset shows the experimental geometry for the $(\frac{1}{2}\,\frac{1}{2}\,14)$ superstructure peak and for fluorescence measurements, while the right inset shows an x-ray Laue pattern of this crystal, viewed along (0 0 L). The incoming beam is polarized horizontally (perpendicular to the scattering plane). (b) Energy scans across the Fe K edge of two superstructure peaks and a regular Bragg peak, indexed in $I4/mmm$. The $(1\,1\,12)_{I4/mmm}$ Bragg peak behaves as expected, with a significant drop in intensity at the resonance followed by a gradual recovery which is due in part to fluorescence. The superstructure peaks exhibit distinct and nontrivial energy dependence.

As can be seen in Fig. S3(b), which references peaks to the $I4/mmm$ cell, the diffraction anomalous fine structure (DAFS) of the superstructure peaks is complex. While the regular tetragonal Bragg peak (1 1 12) shows a characteristic absorption dip at the edge, the two superstructure peaks exhibit a complex energy-dependence throughout the entire edge region. This is related to interference effects between the two Fe sites with dif-

TABLE IV. List of positions probed in reciprocal space referenced to the high-temperature $I4/mmm$ unit cell, together with the peak intensity found there, normalized by incoming beam intensity. Weak peaks were also observed at positions which correspond to intergrowths of the single-layer Ruddlesden-Popper material Sr_2FeO_4 (which are common in Ruddlesden-Popper phases). From the peak intensities, we estimate that these intergrowths occur below one part in 10^4. These peaks were verified to retain their full intensity at 330-350 K, well above the charge order transition in $Sr_3Fe_2O_7$. Based on the l-coordinate and temperature dependence, they can be discriminated from superlattice reflections that belong to $Sr_3Fe_2O_7$. However, some overlap with $Sr_3Fe_2O_7$ reflections is noted in the table. Since this experiment was intended to survey which peaks were present and was not intended to produce quantitative data, readers are cautioned against treating these numbers as quantitative. In particular, a variety of energies and temperatures were used, and some data were collected using an area detector with different sensitivity, as noted in the table. The small beam spot will lead to substantial variations in sample illumination and absorption as a function of the angle between the sample's surface normal and the beam, and, even on a single peak, variations at the 10 % level routinely arise. Peak intensities measured under different conditions should not be compared, and scans along different axes should be treated with caution.

Position	Peak (counts/s)	T (K)	Axis	Energy (eV)	Notes
(0 0 4)	Present	5	z	7112	Area detector
(0 0 6)	9.5×10^{10}	5	θ	7012	
$(\frac{1}{2}\ \frac{1}{2}\ 6)$	6.6×10^{5}	5	L	7112	
$(\frac{1}{2}\ \frac{1}{2}\ 7)$	7.4×10^{5}	5	L	7112	
(1 0 7)	1.8×10^{8}	296	θ	7112	Area detector
(1 1 7)	< 600	6	χ	7012	
$(\frac{1}{2}\ \frac{1}{2}\ 8)$	6.4×10^{5}	5	L	7112	
(1 1 8)	3.9×10^{8}	6	χ	7112	Area detector
$(\frac{1}{2}\ \frac{1}{2}\ 9)$	9.2×10^{5}	5	L	7112	
$(\frac{1}{2}\ \frac{3}{2}\ 9)$	1.8×10^{5}	5	L	7112	
(1 1 9)	< 500	6	χ	7012	
(0 0 10)	1.4×10^{11}	5	χ	7012	
$(\frac{1}{2}\ \frac{1}{2}\ 10)$	1.8×10^{6}	5	L	7112	
$(\frac{1}{2}\ \frac{3}{2}\ 10)$	8.5×10^{5}	5	L	7112	
(1 1 10)	2.1×10^{9}	296	χ	7112	
$(-\frac{1}{2}\ \frac{1}{2}\ 11)$	1.2×10^{5}	5	L	7117	
$(\frac{1}{2}\ \frac{1}{2}\ 11)$	6.6×10^{5}	25	L	7112	
$(\frac{1}{2}\ \frac{3}{2}\ 11)$	3.5×10^{5}	5	L	7112	
(1 1 11)	$< 1.5 \times 10^{5}$	196	L	7112	overlap Sr_2FeO_4 (1 1 7)
$(-\frac{1}{2}\ \frac{1}{2}\ 12)$	8.3×10^{4}	5	L	7117	
(0 0 12)	2.1×10^{10}	5	χ	7012	
(0 1 12)	Absent	5	L	7112	
$(\frac{1}{2}\ \frac{1}{2}\ 12)$	6.2×10^{3}	5	χ	7012	
$(\frac{1}{2}\ \frac{3}{2}\ 12)$	9.5×10^{4}	5	L	7112	
(1 1 12)	2.9×10^{10}	5	χ	7012	
$(1\ 1\ 12\frac{1}{2})$	Absent	5	L	7112	
$(-\frac{1}{2}\ \frac{1}{2}\ 13)$	8.4×10^{5}	5	χ	7112	
(0 0 13)	$< 8.3 \times 10^{5}$	5	χ	7112	overlap Sr_2FeO_4 (0 0 8)
(0 1 13)	3.5×10^{9}	5	χ	7112	
$(\frac{1}{2}\ \frac{1}{2}\ 13)$	7.8×10^{5}	5	χ	7112	
$(\frac{1}{2}\ \frac{3}{2}\ 13)$	2.0×10^{5}	5	χ	7112	
(1 0 13)	4.3×10^{8}	5	χ	7132	
(1 1 13)	$< 2.0 \times 10^{4}$	196	L	7112	overlap Sr_2FeO_4 (1 1 8)
$(0\ 0\ 13\frac{1}{2})$	Absent	5	L	7112	
$(1\ 1\ 13\frac{1}{2})$	Absent	5	L	7112	
$(-\frac{1}{2}\ \frac{1}{2}\ 14)$	1.8×10^{6}	5	L	7117	
(0 1 14)	Absent	5	L	7112	
$(\frac{1}{2}\ \frac{1}{2}\ 14)$	2.3×10^{6}	25	χ	7112	
$(\frac{1}{2}\ \frac{3}{2}\ 14)$	9.0×10^{5}	6	χ	7112	
(1 1 14)	2.2×10^{10}	5	L	7112	
$(1\ 1\ 14\frac{1}{2})$	Absent	5	L	7112	
$(-\frac{1}{2}\ \frac{1}{2}\ 15)$	8.6×10^{5}	5	χ	7112	
(0 1 15)	5.4×10^{10}	5	χ	7112	
$(\frac{1}{2}\ \frac{1}{2}\ 15)$	1.0×10^{6}	25	L	7112	
$(\frac{1}{2}\ \frac{3}{2}\ 15)$	4.1×10^{5}	5	L	7112	
$(0\ 1\ 15\frac{1}{2})$	Absent	5	L	7112	
$(-\frac{1}{2}\ \frac{1}{2}\ 16)$	1.9×10^{5}	5	L	7080	
(0 1 16)	$< 1.0 \times 10^{6}$	196	L	7112	overlap Sr_2FeO_4 (0 1 10)
$(\frac{1}{2}\ \frac{1}{2}\ 16)$	6.2×10^{5}	25	L	7112	
$(\frac{1}{2}\ \frac{3}{2}\ 16)$	2.9×10^{5}	5	L	7112	
$(0\ 1\ 16\frac{1}{2})$	Absent	197	L	7112	
$(-\frac{1}{2}\ \frac{1}{2}\ 17)$	5.4×10^{5}	5	L	7117	
$(\frac{1}{2}\ \frac{1}{2}\ 17)$	9.1×10^{5}	25	L	7112	

ferent valences in combination with the short correlation length along the L direction. The temperature-dependent REXS data presented in the main text were collected at an energy of 7112 eV, or 1.743 Å, corresponding to the dashed vertical line in Fig. S3 just below the pre-edge features. This energy avoids the strong fluorescence background but is close enough to the edge in order to benefit from resonant enhancement. Table IV lists reciprocal-space positions probed by resonant x-ray scattering.

MÖSSBAUER SPECTROSCOPY

Mössbauer spectra were collected between 4.8 and 316 K with a standard WissEl spectrometer, which was operated in constant-acceleration mode and was equipped with a ^{57}Co/Rh source. For the absorber, a crystal of $Sr_3Fe_2O_7$ was ground. The powder containing about 10 mg of natural Fe/cm^2 was diluted with boron nitride to ensure homogeneous distribution and filled into a Plexiglas sample container. In order to prevent sample degra-

dation by moisture the absorber was prepared in an Ar-filled glovebox. Spectra at different temperatures were obtained using a Janis SHI-850-5 closed cycle refrigerator (CCR); the spectra at 292 and 316 K were collected with the CCR switched off. Isomer shifts are given relative to α-Fe. The data were evaluated with the program MossWinn [7] in the perturbation limit $QS \ll B_{hf}$, where QS corresponds to the quadrupole splitting and B_{hf} to the hyperfine field. Spectra were evaluated with Lorentzian-type sextets or with hyperfine field distributions according to the Hesse-Rübartsch method.

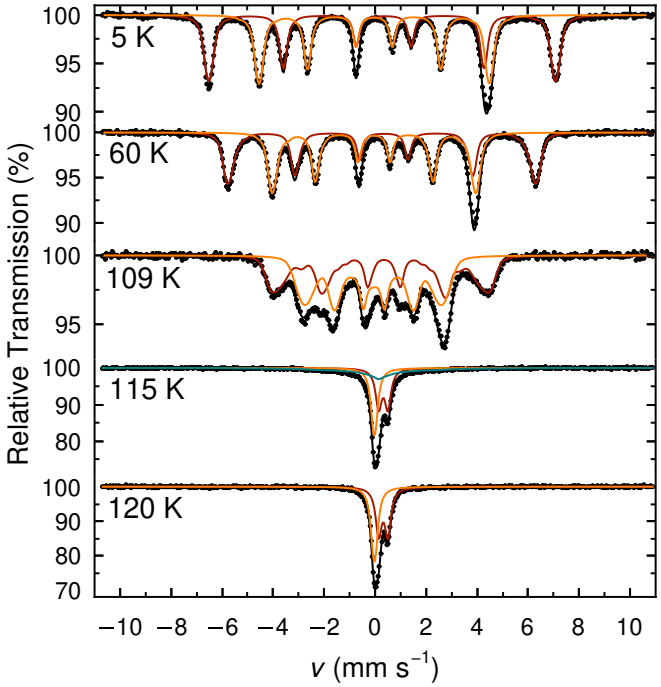

FIG. S4. Mössbauer spectra of $Sr_3Fe_2O_7$ in the magnetically-ordered phase and around the magnetic phase transition. The dark and light components correspond to the "Fe^{3+}" and "Fe^{5+}" sites, respectively. The blue component in the 115-K spectrum reflects the residual magnetically-ordered phase.

Representative Mössbauer spectra of $Sr_3Fe_2O_7$ in the temperature range 5-120 K are shown in Fig. S4, and the isomer shifts IS and hyperfine fields B_{hf} are depicted in Figs. S5 and S6. The spectrum at 5 K can be described by two hyperfine sextets with distinct IS and B_{hf} values which correspond to two inequivalent iron sites. The two sextets are somewhat broadened. Since the line broadening increases with temperature, the spectra were described by two distributions of hyperfine fields, rather than by two distinct sextets with Lorentzian lineshape. The area ratio between the two subspectra is 1:1 which confirms a charge disproportionation (CD) of Fe^{4+}, in agreement with previous investigations of highly-oxidized $Sr_3Fe_2O_7$[8–10].

The CD is frequently written as $2Fe^{4+} \rightarrow Fe^{3+} + Fe^{5+}$. The IS and B_{hf} values are similar to those in $CaFeO_3$

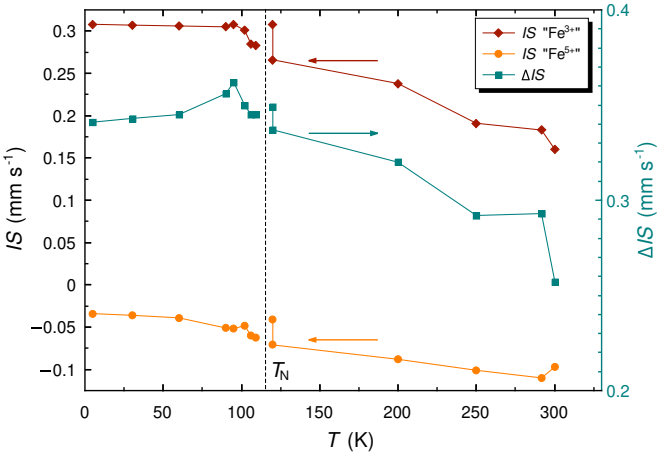

FIG. S5. Temperature dependence of the isomer shifts IS of the "Fe^{3+}" (dark) and "Fe^{5+}" (light) sites and of the difference ΔIS of the isomer shifts between the two sites (green). The solid lines are guides to the eye.

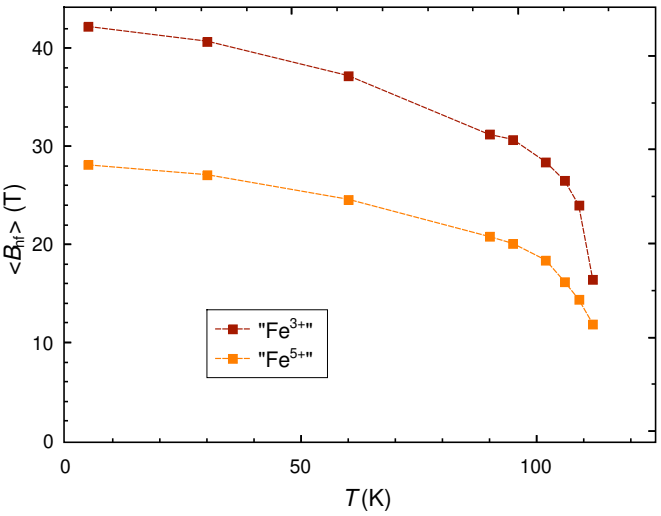

FIG. S6. Temperature dependence of the average hyperfine fields $\langle B_{hf} \rangle$ of the "Fe^{3+}" (dark) and "Fe^{5+}" (light) sites. The data were obtained by evaluation of the spectra with a distribution model. The Néel temperature was chosen to be 115.0 K, although a minor fraction is still in the magnetically ordered phase. The dashed lines are guides to the eye.

[11] which is the classical example for a CD of Fe^{4+}. However, as pointed out previously[9], the IS of 0.31 mm/s at 5 K for the "Fe^{3+}" site is considerably smaller than the typical values of ~0.45 mm/s for Fe^{3+} in octahedral oxygen coordination, whereas the $IS = -0.03$ mm/s for "Fe^{5+}" is larger than for instance $IS = -0.34$ mm/s found in the Fe^{5+} double perovskite La_2FeLiO_6[12]. Similarly, the hyperfine fields of 42 and 28 T are smaller and larger than expected values of >50 T for Fe^{3+} and 23 T for Fe^{5+}, respectively[12]. Accordingly, the differences ΔIS and ΔB_{hf} in isomer shifts and hyperfine fields between the two species are smaller than expected for a full

charge disproportionation, which is in qualitative agreement with the view that these formal iron(IV) oxides are strongly covalent and can be considered as negative-Δ materials[13], where Δ is the charge-transfer energy. Then the CD may be formulated as $2\,d^5\mathrm{L}^{-1} \rightarrow d^5 + d^5\mathrm{L}^{-2}$, where L^{-1} and L^{-2} represent one and two holes in the oxygen coordination sphere, respectively. The formulation $2\mathrm{Fe}^{4+} \rightarrow \mathrm{Fe}^{(4-\delta)+} + \mathrm{Fe}^{(4+\delta)+}$ has also been used to indicate an incomplete degree of charge separation. In any case, the CD clearly alters the electron and spin densities at the iron sites which gives rise to distinct IS and B_{hf} values. As there is only a small quadrupole interaction, the different B_{hf}s correspond to different ordered magnetic moments at the two sites. For $CaFeO_3$, ordered magnetic moments of 3.5 and 2.5 μ_B were obtained from neutron diffraction studies for the helical state of $CaFeO_3$[14]. Since the B_{hf} values of $CaFeO_3$ are quite similar to those of $Sr_3Fe_2O_7$, similar moments are expected. The difference ΔIS is also nearly the same in the two compounds, which implies a comparable degree of charge segregation in $Sr_3Fe_2O_7$ and $CaFeO_3$.

The CD remains nearly unchanged up to the magnetic ordering temperature T_N ~115 K, where phase coexistence of the paramagnetic and magnetically-ordered phases is found. The latter appears as a broad magnetic hyperfine pattern which is superimposed on the paramagnetic subspectrum. In the magnetically-ordered phase the spectra become continuously broadened with increasing temperature which is reflected in an increased distribution width of B_{hf}. The broadening could reflect slight variations of the magnetic ordering temperature due to a residual oxygen deficiency and/or spin fluctuations. It is noteworthy that even at 5 K a broadening is observed which is more pronounced for the "Fe^{3+}" subspectrum than for the "Fe^{5+}" subspectrum. This may reflect the helical spin structure of $Sr_3Fe_2O_7$[15]. The "Fe^{3+}" site has a larger quadrupole splitting than the "Fe^{5+}" site, where the quadrupole interaction essentially vanishes. The quadrupole splitting parameter QS for "Fe^{3+}" (−0.06 mm/s at 5 K) depends on the angle between the principal axis V_{ZZ} of the electric field gradient (efg) and the spin direction, which varies in the case of a helical spin structure. The resulting distribution in QS may be the origin of the increased broadening in the case of the "Fe^{3+}" component.

At 120 K the sample is completely in the paramagnetic state. It is obvious that the spectra between 120 and 316 K (Fig. S7) are composed of two components, which evidences that the CD persists in the paramagnetic phase. The spectra were described by two quadrupole doublets, with quadrupole splitting QS of 0.07 and 0.36 mm/s at 120 K for the "Fe^{5+}" and "Fe^{3+}" sites, respectively. Thus, the "Fe^{5+}" component is essentially a slightly broadened single line. The temperature dependence of the isomer shifts and of the difference between the isomer shifts ΔIS of the two sites in both

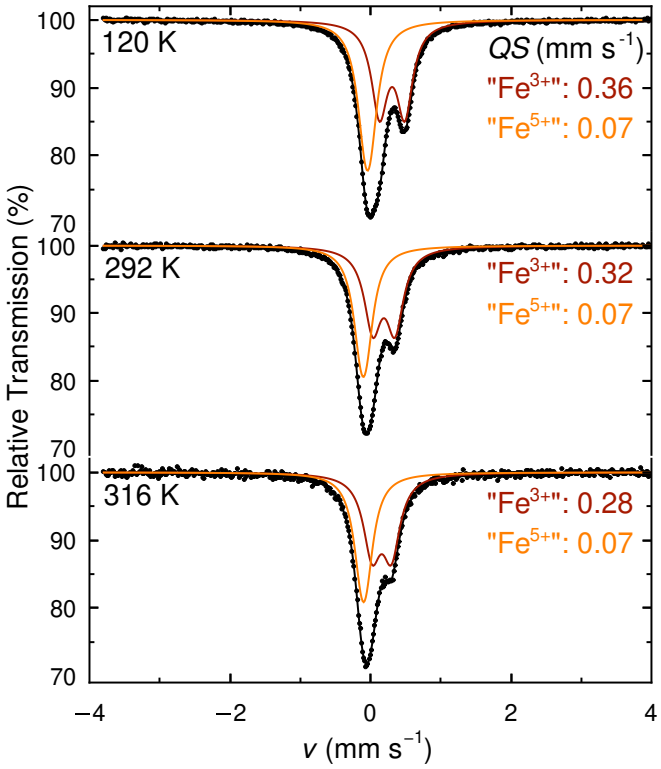

FIG. S7. Mössbauer spectra of $Sr_3Fe_2O_7$ in the paramagnetic phase. The dark and light components correspond to the "Fe^{3+}" and "Fe^{5+}" sites, respectively. The values QS of the quadrupole splitting are given in the figure.

the magnetically ordered and the paramagnetic phase is shown in Fig. S5. In agreement with the earlier results these data suggest that the CD is largely insensitive to the magnetic phase transition. With increasing temperature, in particular above 200 K, ΔIS decreases, which indicates that the degree of charge separation is reduced[9], an effect which is also visible in the resonant diffraction results in the main text. Nevertheless, the CD is still apparent at 316 K, the highest temperature in this study. This is in agreement with the results in the main text and with the slightly higher $T_\mathrm{CO} = 343\pm10$ K reported in Ref. 10.

We note that the fit of the spectra in the paramagnetic phase is not unique, and there is another fit with somewhat increased values of QS for both the "Fe^{3+}" and the "Fe^{5+}" sites which reproduces the spectra equally well. This data analysis, however, results in an anomaly in ΔIS near the magnetic phase transition and thus would point to a magnetostriction effect, which reduces the charge segregation at T_N. A magnetostriction effect is, however, excluded by the neutron Larmor diffraction results in the main text, and thus this fit is discarded.

In summary, the Mössbauer study on the present $Sr_3Fe_2O_7$ sample corroborates the CD of Fe^{4+} and is fully consistent with the crystal structure data at 15 K

which reveal a bond-length alternation within in the double layers. The Fe1 sites with the larger bond distances correspond to the "Fe^{3+}" sites in the Mössbauer spectra, whereas the Fe2 sites correspond to the contracted "Fe^{5+}" sites.

* These authors contributed equally to this work.
† b.keimer@fkf.mpg.de

[1] D. C. Peets, J.-H. Kim, P. Dosanjh, M. Reehuis, A. Maljuk, N. Aliouane, C. Ulrich, and B. Keimer, Magnetic phase diagram of $Sr_3Fe_2O_{7-\delta}$, Phys. Rev. B **87**, 214410 (2013).

[2] A. Maljuk, J. Strempfer, C. Ulrich, M. Sofin, L. Capogna, C. Lin, and B. Keimer, Growth of $Sr_3Fe_2O_{7-x}$ single crystals by the floating zone method, Journal of Crystal Growth **273**, 207 (2004).

[3] S. R. Hall, G. S. D. King, and J. M. Stewart, eds., *The* XTAL3.4 *User's Manual* (Lamb Print, University of Western Australia, Perth, 1995).

[4] E. Prince, ed., *International Tables of Crystallography*, Vol. C (International Union of Crystallography, 2006).

[5] J. Rodríguez-Carvajal, Recent advances in magnetic structure determination by neutron powder diffraction, Physica B: Condensed Matter **192**, 55 (1993).

[6] J. Strempfer, S. Francoual, D. Reuther, D. K. Shukla, A. Skaugen, H. Schulte-Schrepping, T. Krachta, and H. Franz, Resonant scattering and diffraction beamline P09 at PETRA III, Journal of Synchrotron Radiation **20**, 541 (2013).

[7] Z. Klencsár, MOSSWINN—methodological advances in the field of Mössbauer data analysis, Hyperfine Interactions **217**, 117 (2013).

[8] S. E. Dann, M. T. Weller, D. B. Currie, M. F. Thomas, and A. D. Al-Rawwas, Structure and magnetic properties of Sr_2FeO_4 and $Sr_3Fe_2O_7$ studied by powder neutron diffraction and Mössbauer spectroscopy, J. Mater. Chem. **3**, 1231 (1993).

[9] P. Adler, Electronic state, magnetism, and electrical transport behavior of $Sr_{3-x}A_xFe_2O_7$ ($x \leq 0.4$, A = Ba, La), Journal of Solid State Chemistry **130**, 129 (1997).

[10] K. Kuzushita, S. Morimoto, S. Nasu, and S. Nakamura, Charge disproportionation and antiferromagnetic order of $Sr_3Fe_2O_7$, Journal of the Physical Society of Japan **69**, 2767 (2000).

[11] M. Takano, N. Nakanishi, Y. Takeda, S. Naka, and T. Takada, Charge disproportionation in $CaFeO_3$ studied with the Mössbauer effect, Materials Research Bulletin **12**, 923 (1977).

[12] G. Demazeau, B. Buffat, F. Ménil, L. Fournès, M. Pouchard, J. M. Dance, P. Fabritchnyi, and P. Hagenmuller, Characterization of six-coordinated iron (V) in an oxide lattice, Materials Research Bulletin **16**, 1465 (1981).

[13] A. E. Bocquet, A. Fujimori, T. Mizokawa, T. Saitoh, H. Namatame, S. Suga, N. Kimizuka, Y. Takeda, and M. Takano, Electronic structure of $SrFe^{4+}O_3$ and related Fe perovskite oxides, Phys. Rev. B **45**, 1561 (1992).

[14] P. M. Woodward, D. E. Cox, E. Moshopoulou, A. W. Sleight, and S. Morimoto, Structural studies of charge disproportionation and magnetic order in $CaFeO_3$, Phys. Rev. B **62**, 844 (2000).

[15] J.-H. Kim, A. Jain, M. Reehuis, G. Khaliullin, D. C. Peets, C. Ulrich, J. T. Park, E. Faulhaber, A. Hoser, H. C. Walker, D. T. Adroja, A. C. Walters, D. S. Inosov, A. Maljuk, and B. Keimer, Competing exchange interactions on the verge of a metal-insulator transition in the two-dimensional spiral magnet $Sr_3Fe_2O_7$, Phys. Rev. Lett. **113**, 147206 (2014).